RSC Advances

ROYAL SOCIETY OF CHEMISTRY

www.rsc.org/advances

Journal Name

RSCPublishing

ARTICLE

Cyclic RGD targeting cisplatin micelles for near-infrared imaging-guided chemotherapy

Cite this: DOI: 10.1039/x0xx00000x

Xingang Guan,[a,b] Xiuli Hu,[b] Shi Liu[b], Xin Sun[a,*] and Xiaodong Gai[c,*]

Received 00th January 2012,
Accepted 00th January 2012

DOI: 10.1039/x0xx00000x

www.rsc.org/

Nowadays imaging-guided chemotherapy has been of great importance for developing high efficient nanomedicines for cancer therapy. However, the drug accumulation and release in vivo can not be tracked in most studies due to the imaging moiety. In this study, near-infrared (NIR) dyes, cisplatin and dextran were used to prepare a imaging-guided chemotherapy drug with cyclic peptide arginine-glycine-aspartic acid (RGD) targeting property in treatment of breast cancer. Confocal laser scanning microscopy (CLSM) analysis indicated that the cisplatin-loaded micelles with cRGD decoration were quickly uptaked by breast cancers cells in vitro according to the fluorescence of NIR dye. More importantly, in vivo bioluminescence imaging analysis indicated that the drug-loaded micelles were preferentially distributed in tumor regions of tumor-bearing mice. Furthermore, combining RGD targeting, in vivo imaging and therapeutic property, this nanomedicine suggested a good anti-tumor activity in vivo. Our study highlights the potential of combining active targeting and NIR fluorescence imaging in one drug delivery system for cancer diagnosis and therapy.

1 Introduction

Multifunctional nanoparticles for tumor imaging, cell targeting and anti-cancer drug delivery have attracted a great deal of attention for cancer therapy.[1-4] The nanoparticles were designed to be equipped with several moieties to optimize the treatment of cancer. For example, targeting moieties can improve drug accumulation in certain tumors, imaging moieties can be used to analyze the drug biodistribution in vitro or in vivo, microenvironmental sensors (pH, redox, oxygen, proteases, and temperature) which triggered drug release in tumors reduced the damage of normal tissues.[5-7] These nanoparticles can not only selectively accumulate in certain tumors which could be observed via imaging moieties, but also release chemotherapy drugs to cancer cells to perform therapeutic function.[8-11] The all-in-one systems hold great promise for cancer therapy.

Polymeric micelles have attracted widespread interest in anti-cancer drug delivery because of their hydrophobic core.[12-16] Until now, various types of materials have been used to prepare block copolymer which can self-assemble into nanoparticles for drug delivery.[17-19] Among these materials, dextran has been considered as a good candidate due to their excellent biocompatibility and degradability.[20,21] By introduction of hydrophobic building block, the drug-loaded dextran micelles showed enhanced cell uptake, superior antitumor activity than small molecular drugs.[22-24]

4,4-Difluoro-4-borata-3a,4a-diaza-*s*-indacene (BODIPY, BDP) has been widely used in bioimaging and diagnostics area due to its excellent characteristics including environmentally robust fluorescence, high photostability and brightness, and favorable cell permeability.[25-28] BODIPY dyes whose emission maximum located in the far-red and near-infrared (NIR) (650–900 nm) are preferred in biomedical imaging because of deep tissue penetration and high signal-to-noise ratio.[29, 30] In this study, the NIR BODIPY (Ex_{max}=590 nm, Em_{max}=673 nm) grafted dextran were used to prepare micelles for imaging-guided chemotherapy. The drug distribution and release could be obtained real-time by optical imaging system. In addition, cyclic peptide arginine-glycine-aspartic acid (RGD) which could selectively bind with $\alpha_v\beta_3$ and $\alpha_v\beta_5$ integrins was utilized to deliver cisplatin (CDDP) to breast cancers.[31-33] Cisplatin, a famous antitumor drug widely employed in cancer chemotherapy, was loaded through the complexing with carboxyl groups of dextran.[34-36]

In this study, the CDDP release, the cellular uptake and cytotoxicity of nanoparticles in vitro, the imaging and treatment of cancer in vivo were evaluated in detailed.

2 Material and Methods

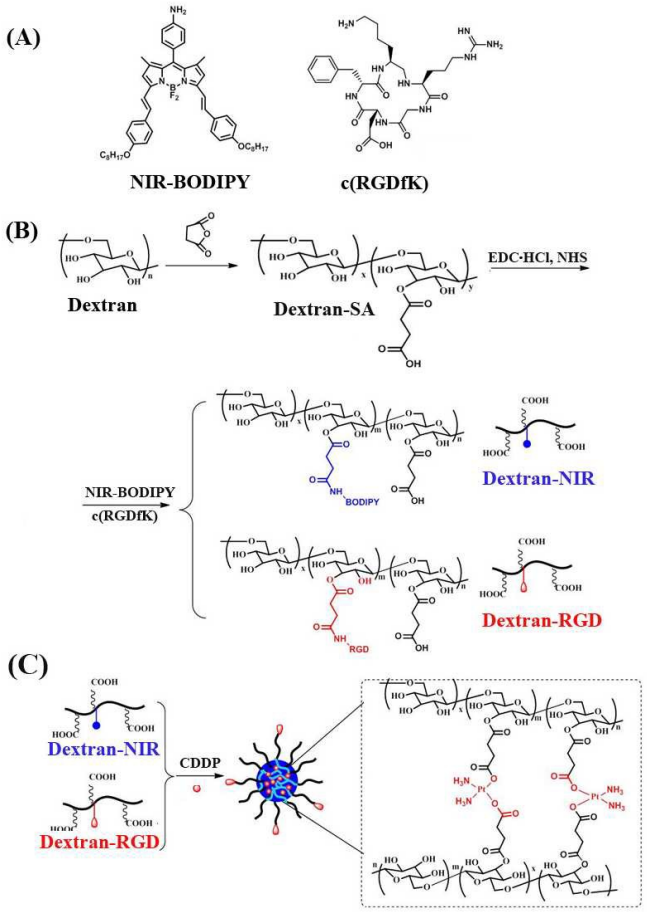

Scheme 1 (A) The chemical structure of NIR BODIPY and RGD; (B) the synthesis of dextran-NIR and dextran-RGD; (C) preparation of cisplatin micelles.

2.1 Synthesis of near-infrared BODIPY dye

The synthesis of BODIPY was reported by our laboratory.[37] Its chemical structure was shown in Scheme 1. The UV-vis absorption and fluorescence emission was tested to be 643 and 673 nm in dimethylformamide (DMF), respectively.

2.2 Synthesis of dextran derivatives with succinic anhydride (dextran-SA)

Dextran (1 g, 6.17 mmol) was dissolved in 6 mL of dry DMSO in a flame-dried flask, followed by addition of 4-(dimethylamino) pyridine (DMAP, 754 mg, 6.17 mmol) solution in DMSO (2 mL) and succinic anhydride (SA, 617 mg, 6.17 mmol) in DMSO (2 mL), respectively. The reaction was performed at 50°C for 24 h under nitrogen. The product was isolated by precipitation in cold ethanol, washed several times with ethanol, and dried under vacuum. The resulting white powder was then dissolved in deionized water, dialyzed for 48 h to remove the excess reactants. The final product was obtained as a white powder after lyophilization (Yield: 96%).

2.3 Synthesis of dextran-RGD and dextran-BDP

For dextran-RGD synthesis, 500 mg (50 μmol) Dextran-SA, 14.4 mg (75 μmol) 1-ethyl-3-(3-dimethylaminopropyl) carbodiimide hydrochloride (EDC) and 16.3 mg (75 μmol) N-hydroxysulfosuccinimide (Sulfo-NHS) were dissolved in 10 mL deionized water, and the pH value of the solution was adjusted to 5.4. The reaction was conducted at room temperature for 2 h and then 30 mg (50 μmol) RGD peptide was added. After 12 h of reaction, the solution was dialyzed against distilled water for 12 h (MWCO=3500), the final suspension in dialysis bag containing RGD-Dextran was freeze-dried. The RGD peptide content of the polymers was determined by measuring the arginine content as reported in the reference.[38]

Dextran-BDP was synthesized as below. 100 mg of dextran (0.38 mmol COOH) was dissolved in 10 mL of DMSO, and 3.6 mg of EDC·HCl (2.4 mg) and 1.4 mg of NHS were added at 0 °C and stirred for 12 h, then 9.5 mg of BDP (0.012 mmol) was added and stirred for an additional 12 h. the reaction product was dialyzed against distilled water for 12 h (MWCO=3500) and freeze-dried. The BDP content of the obtained dextran-BDP was determined by UV-Vis spectrometer.

2.4 Preparation of BDP conjugated dextran-cisplatin complex micelles (M(BDP/Pt)) and RGD decorated micelles (RGD-M(BDP/Pt))

The synthesis of cisplatin-dextran complex micelles was described in the literature.[39] 0.1 g of cisplatin was suspended in 10 mL distilled water and mixed with 0.113 g silver nitrate ($AgNO_3$/cisplatin=2 mol/mol). After stirring in the dark for 4 h at room temperature, the AgCl precipitates were removed by filtration. The filtrate was used directly. The mixture of dextran-SA and dextran-BDP (40 mg with weight ratio of 1:1) was dissolved in 4 mL deionized water, and then 7.5 mg Na_2CO_3 were added to deprotonate the carboxyl groups. Different amounts of silver nitrate were added to the solution and stirred for 2 h in the dark, and then the solution was dialyzed (cutoff = 3500) against deionized water for 10 h to remove unreacted cisplatin. The obtained micelles were abbreviated as M(BDP/Pt).

RGD decorated micelles were prepared similarly by adding 20 wt% dextran-RGD in the mixture polymer for drug complex. These micelles were abbreviated as RGD-M(BDP/Pt).

The BDP content of in the micelles were measured by UV-Vis spectrometer and the cisplatin-loading content (LC) and encapsulation efficiency (EE) were determined by ICP-OES. The LC and EE were calculated according to the following formula:

LC % = weight of loaded drug×100/ weight of loaded drug+ weight of polymer used;

EE % = weight of loaded drug×100/weight of feeding drug.

2.5 Characterization of polymer micelles

The morphology of polymer micelles was determined by transmission electron microscope (TEM) (JEOL JEM-1011 electron microscope). Size and size distribution of micelles was measured by dynamic light scattering (DLS) with a vertically

polarized He–Ne laser (DAWN EOS, Wyatt Technologies). The scattering angle was fixed at 90° for DLS measurement at 25 ℃.

2.6 Cell viability assay

Mouse mammary carcinoma (EMT6) cells were seeded in 96-well plates at a density of 4×10^3 cells/well in 100 μL Dulbecco's modified Eagle's medium (DMEM) containing 10 % fetal bovine serum (FBS) for 12 h at 37 ^oC in 5 % CO_2. The medium was replaced with 200 μL DMEM medium containing different concentrations of polymers (dextran-SA: dextran-BDP =1:1) ranged from 100 to 1000 μg/mL for 48 h. 20 μL MTT (5 mg/mL) was added to each well for 4 h incubation, and then 150 μL DMSO were added to each well to dissolve the blue formazan formed in the live cells. The absorbance was measured on a microplate reader (BioTek, EXL808) at 490 nm. Experiments were repeated three times.

2.7 In vitro cisplatin release

The release profile of cisplatin from M(BDP/Pt) micelles at different pH values (pH 7.4 and pH 5.0) were tested by dialysis method. Briefly, the weighted freeze-dried M(BDP/Pt) was suspended in 5 mL of release medium and transferred into a dialysis bag (cutoff=3500) and sealed. The release experiment was initiated by placing the sealed dialysis bag into 20 mL of release medium (20 mM PBS, pH 7.4 and pH 5.0) at 37^oC with shaking. At selected time intervals, 1 mL of release media was taken out and replenished with an equal volume of fresh media. The amount of Pt released was measured by ICP-OES, and the cumulative Pt release percentage was calculated and plotted against the release time.

2.8 The subcellular localization in cancer cells

The subcellular localization of M(BDP/Pt) micelles and RGD-M(BDP/Pt) micelles were observed by confocal laser scanning microscopy (CLSM). Briefly, 1×10^5 EMT6 cells per well were seeded onto cover slides in six-well plate and incubated for 12 h. The medium was replaced with 2 mL fresh medium containing 20 μg BDP for 1, 3, 6, 9, 12, 24 h, respectively. The cells were washed three times with PBS, and fixed with 4 % (w/v) paraformaldehyde for 15 min at room temperature. The cells were counterstained with 4, 6-diamidino-2-phenylindole (DAPI) for cell nucleus. The cellular localization was visualized under a confocal laser scanning microscope (Carl Zeiss LSM 780).

In order to investigate whether dextran-NIR micelles escaped form endosomes, late endosome and lysosome specific probe was used in co-localization analysis. The cell seed and fixed process was the same as above mentioned. After fixing with 4 % (w/v) paraformaldehyde, the cells were staining with LysoTracker Red (Beyotime Institute of Biotechnology, 50 nM) for 30 min and washed with PBS for three times. DAPI was excited with a blue diode (405 nm) and detected in the 415–460 nm range. Lyso-tracker were excited with a laser (555 nm) and detected in the 570–590 nm range. NIR BODIPY was excited in 633 nm and detected in the 650–775 nm range. CLSM images were captured via confocal microscope under the same parameters.

2.9 Cytotoxicity of M(BDP/Pt) and RGD-M(BDP/Pt)

The cytotoxicity test was conducted to examine the antitumor activity of free cisplatin, M(BDP/Pt) and RGD-M(BDP/Pt) via 3-(4, 5-dimethylthiazol-2-yl) 2, 5-diphenyl tetrazolium bromide (MTT) assay. Briefly, 4000 cells per well were seeded to 96 well plate and incubated for more than 12 h. The medium was refreshed with 200 μL DMEM medium containing different concentrations of Pt or micelles for 48 h. The Pt concentration ranged from 0.01 to 50 μg/mL. 20 μL MTT (5 mg/mL) was added to each well and incubation was continued for more 4 h, and then 150 μL DMSO were added to each well to dissolve the blue formazan formed in the live cells. The absorbance was measured on a microplate reader at 490 nm. Experiments were repeated three times.

2.10 Biodistribution of micelles in vivo

All animals were performed in compliance with the guidelines established by Animal Care and Use Committee of Beihua University, and all procedures were approved by the Animal Care and Use Committee of Beihua University. Ten BALB/C mice were utilized to implant xenograft EMT6 mouse mammary carcinoma. To develop the tumor xenograft, 1 million EMT6 cells were injected to lateral aspect of anterior limb of the mice. After tumor volume reached 50~100 mm^3, xenograft-bearing mice were divided randomly into 2 groups: M-(BDP/Pt) and RGD-M(BDP/Pt) micelle groups. M-(BDP/Pt) and RGD-M-(BDP/Pt) micelles were injected to xenograft-bearing mice via a tail vein, respectively (with an equivalent BDP dose of 30 μg). The fluorescence observations were carried out 8, 12 and 24 h after vena tail injection by imaging system. The imaging system (CRI Maestro 500FL) used in this study consisted of a light-tight box equipped with a 150 W halogen lamp and an excitation filter system (575-605 nm) to excite NIR BODIPY. Fluorescence was detected by a CCD camera equipped with a C-mount lens and an emission filter (Longpass: 645 nm cut-in).

2.11 Anti-tumor efficacy

All animals were performed in compliance with the guidelines established by Animal Care and Use Committee of Beihua University, and all procedures were approved by the Animal Care and Use Committee of Beihua University.The in vivo anti-tumor efficacy of the drug-loaded micelles was evaluated using the xenograft EMT6 mouse mammary carcinoma implanted on BALB/C mice. When tumor volume of the mice reached 30~70 mm^3, and this day was designated as day 0. The mice were weighed and randomly divided into 4 groups (5 mice per group): saline, free cisplatin, M-(BDP/Pt) and RGD-M-(BDP/Pt) micelles (dosage: 5 mg Pt equivalent/kg body weight). The drug injection was carried out on day 0, 2, 4 via tail vein. The anti-tumor efficacy evaluation were assessed by measuring the tumor volume. The anti-tumor activities were evaluated by measuring the tumor volume (V) estimated by the following

equation: $V = ab^2/2$, where a and b stand for the major and minor axes of the tumor measured via vernier micrometer.

2.12 Statistics

All experiments were performed at least three times and all results are expressed as mean±SD (standard deviation). Students't-test was used to demonstrate statistical significance ($P<0.05$).

3 Results and discussion

To endow micelles active targeting and bioimaging property simultaneously, cyclic RGD peptide and BODIPY dye were conjugated to the dextran in this study. The chemical structure of BODIPY and RGD were shown in Scheme 1(A). Scheme 1(B) gives the synthesis process of dextran-RGD and dextran-NIR and Scheme 1(C) is the schematic illustration of RGD targeting cisplatin micelles complex with dextran.

3.1 Modification of dextran

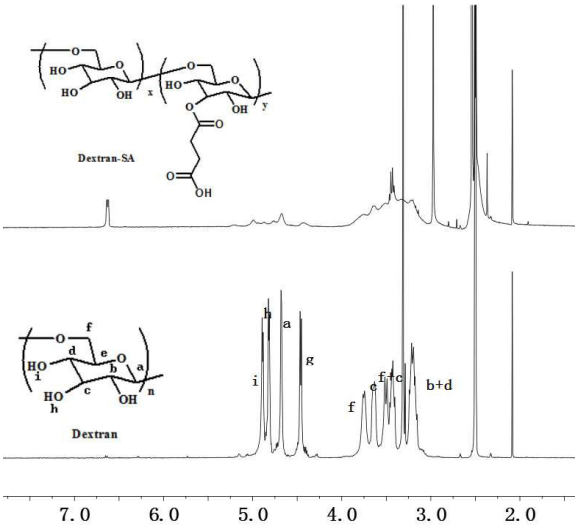

Fig. 1 ^{1}H NMR spectra of dextran and dextran-SA.

The synthesis of dextran-SA was according to the literature with high yield (>95%). The ^{1}H NMR of dextran and dextran-SA was shown in Fig. 1. The introducing side carboxyl groups provided sites for further functionalization.

We had synthesized a highly hydrophobic BODIPY dye and investigated its off-on fluorescent properties by conjugating with mPEG to form nanovesicles.[37] Similarly, in this paper, we conjugated BODIPY onto dextran side groups and the formed dextran micelles have off-on fluorescent properties. BODIPY moieties in the micelles are in the aggregated state and thus fluoresce weakly due to the aggregation quenching effect. Once the micelles entered into the cells and micelles are dissociated, the NIR dyes become intensely fluorescent. [37] The synthesis process of dextran-NIR was shown in Scheme 1(B) and the BODIPY content in dextran-NIR was determined to be 6.7% (wt/wt) by UV-vis spectrometer.

The cyclic RGD was selected as an active targeting moiety and was conjugated to dextran as shown in Scheme 1(B). The molar ratio of cRGD peptide to dextran was determined to be 56.4% by measuring the arginine content using the reported method.[38]

3.2 Preparation of M(BDP/Pt) and RGD-M(BDP/Pt) micelles

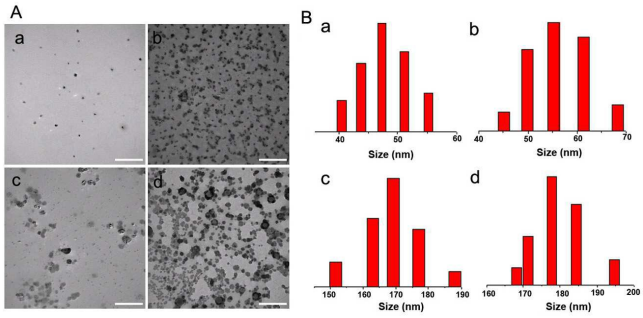

Fig. 2 Characterization of different polymer micelles by TEM (A) and DLS (B) analysis. a: M(Pt); b:RGD-M(Pt); c: M(BDP/Pt); d: RGD- M(BDP/Pt). Scale bar: 500 nm.

The residual carboxyl groups in dextran-RGD and dextran-NIR can be used to coordinate with cisplatin. Three kinds of polymers (dextran-SA, dextran-RGD, and dextran-NIR) were used to prepare micelles. With the increase of CDDP feed ratio, the DLC and mean diameter of micelles increased gradually, while zeta potentials were decreased, which may be attributed to the consumption of carboxyl groups while complex with cisplatin. To find a balance between the CDDP loading and the size of polymer micelles, in this study 15% of CDDP were used to prepare our all-in-one micelles.

Functionalized micelles were prepared by adding dextran-RGD or dextran-NIR or both of them to the polymer. 20 wt % of RGD conjugated polymer in the mixture was selected according to our previously study. The prepared micelles were characterized by TEM and DLS as shown in Fig. 2. The results showed that all micelles displayed spherical structure. The diameter of M(Pt), RGD-M(Pt), M(BDP/Pt) and RGD-M(BDP/Pt) were 48, 55, 169 and 177 nm, respectively. After adding RGD decoration, the particle sizes increased about 6 or 7 nm.

3.3 Drug release in vitro and biocompatibility analysis

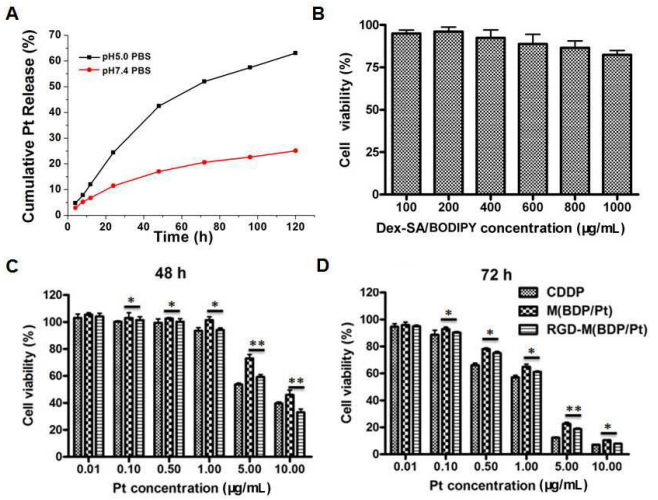

Fig. 3 Drug release in vitro, cell viability analysis and cytoxicity of Pt-loaded micelles. A: In vitro cumulative release profiles of Pt from M(BDP/Pt) at different pHs (pH 5.0 and 7.4) at 37 ℃; B: Biocompatibility assay of polymers (Dex-SA/NIR); C and D: The cytotoxicity of CDDP, M(BDP/Pt) and RGD-M(BDP/Pt) were measured after incubation with EMT6 cells for 48 (C) and 72 h (D) by MTT assays. All the results are average of three measurements, and list as mean±SD.

The release of Pt from M(BDP/Pt) was investigated in PBS buffers (pH 5.0 and pH 7.4). The released Pt was determined by ICP-OES. As shown in Fig. 3A, sustained release of Pt were observed in PBS buffers within 120 h. However, 63 % of Pt was released in pH 5.0 PBS at 120 h, while only 25 % Pt release was detected in pH 7.4 PBS. The biocompatibility of nanomaterials is very important for their biomedical application.[40] In vitro biocompatibility of Dex-SA/NIR (Dex-SA:Dex-NIR=1:1) against EMT6 cells at 48 h were performed at different concentration. As shown in Fig. 3B, the cell viability was more than 82 % at all test concentrations up to 1 mg/mL, indicating good compatibility of the polymers with the EMT6 cells.

In order to examine the cytotoxicity of our micelles, MTT analyses were performed on EMT6 cells at different concentrations (0.01~10 μg/mL). The survival rates of EMT6 cells after incubation with free CDDP, M(BDP/Pt) and RGD-M(BDP/Pt) for 48 h were examined. As shown in Fig. 3C and 3D, the cell viability treated with RGD-M(BDP/Pt) was much lower than that of M(BDP/Pt) at most drug concentrations, which may be ascribed to much more cell uptake of RGD-decorated micelles than untargeted micelles. Moreover, 67 % cells treated with RGD-M(BDP/Pt) were killed at a concentration of 10 μg/mL, which was even higher than the 60% of free CDDP. These results suggest that our dextran micelles have good biocompatibility and stronger cytotoxicity than free CDDP.

3.4 Cellular uptake

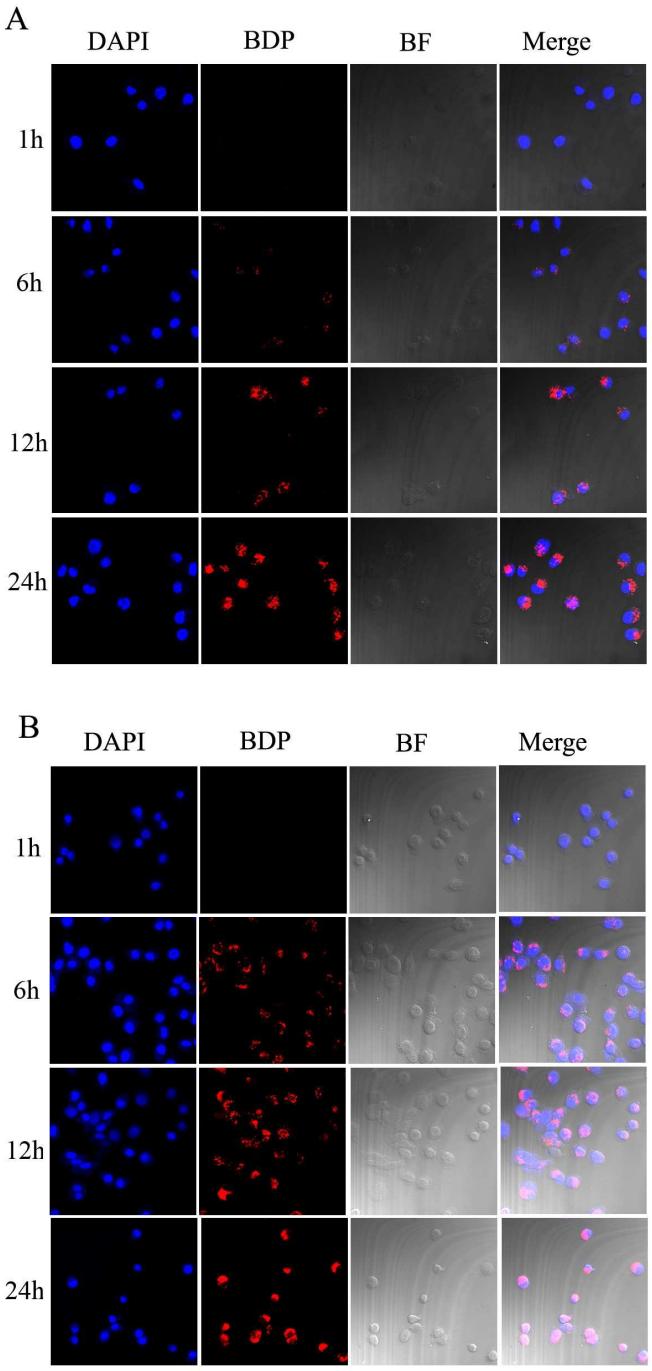

Fig. 4 CLSM images of the EMT6 cells after 1, 6, 12 and 24 h of incubation with the M(BDP/Pt)(A) or RGD-M(BDP/Pt)(B). The cellular nuclei was stained by DAPI (blue), BODIPY fluorescence was indicated as red, BF represents bright field, and Merge means the overlays of three images.

The cellular uptake of RGD-M(BDP/Pt) and M(BDP/Pt) were examined by measuring the fluorescence of BDP (excitation wavelength: 633 nm) by CLSM. As shown in Fig. 4, the fluorescence cannot be observed until 6 h incubation of M(BDP/Pt) and the fluorescence intensity from BODIPY increased gradually by prolonging the incubation time from 6 h to 24 h. As for RGD-M(BDP/Pt) micelles, the BDP

fluorescence could be detected after 3h of incubation (not shown), which appeared even brighter than that in EMT6 cells incubated with M(BDP/Pt) for 6 h. As reported by many reports,[41] RGD targeted nanoparticles could be internalized via receptor mediated endocytosis, which is much faster than that of untargeted controls. So the faster BDP release in RGD-M(BDP/Pt) group may be attributed to the different pathway of endocytosis between M(BDP/Pt) and RGD-M(BDP/Pt).

The above results indicated a positive correlation between fluorescence intensity and incubation time for both micelles. In consideration of the self-quenching property of our NIR BDP at high concentration, the higher fluorescence intensity could be an evidence for more BDP release from micelles.

3.5 Co-localization with lysosomes

To investigate whether micelles escaped from endosomes, the late endosomes and lysosomes were stained by Lyso-Tracker in this study. As shown in Fig. 5, merging of yellow fluorescence could be observed after 6 h incubation of M(BDP/Pt) or 3 h of RGD-M(BDP/Pt). The merged yellow fluorescence clearly demonstrated co-localization of micelles with endosomes, suggesting a potential endosomes escape. As the incubation time prolonged to 24 h, the intensity of yellow fluorescence reached a maximum. These results indicated that RGD-M(BDP/Pt) efficiently enhanced the endosomal escape in EMT6 cells compared with M(BDP/Pt).

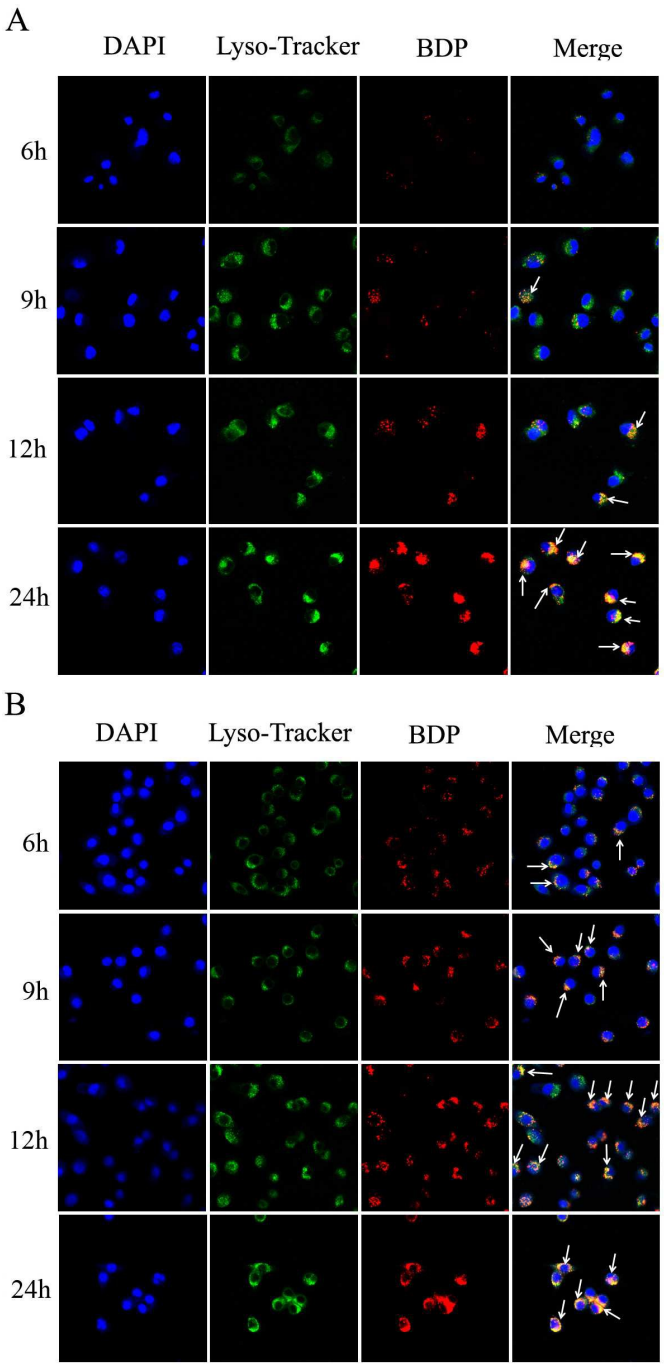

Fig. 5 CLSM images of EMT6 cells incubated for 6, 9, 12 and 24 h with M(BDP/Pt)(A) or RGD-M(BDP/Pt)(B). The late endosomes and lysosomes were stained with LysoTracker (green). The cell nucleus was stained by DAPI (blue), and the red fluorescence was emitted by BDP. The yellow fluorescence, which was generated by overlay of green and red fluorescence was indicated as arrows.

3.6 Distribution of micelles in vivo

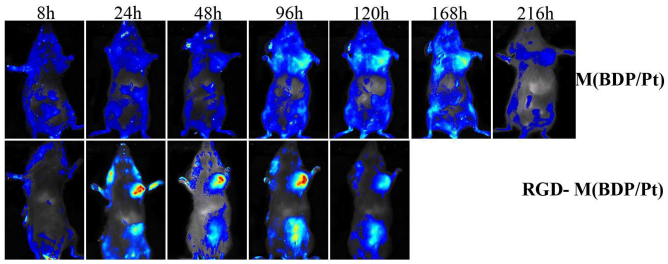

Fig. 6 The BDP releases in vivo were visualized after vena tail injection using CRI Maestro 500FL imaging system.

To examine the distribution of M(BDP/Pt) and RGD-M(BDP/Pt) in vivo, equal BDP dose of micelles (30 μg) were administered via tail vein injection. As shown in Fig. 6, for M(BDP/Pt) group the fluorescence in tumor cannot be detected until 48 h after injection, and the peak intensity of fluorescence was observed 168 h after injection; however, a high BDP fluorescence in mice injected with RGD-M(BDP/Pt) could be detected within 24 h injection, and the fluorescence reached its maximum at 96 h after injection. These results indicated that the BODIPY release from M(BDP/Pt) micelles was delayed for 24 h to 48 h compared with that of RGD-M(BDP/Pt) micelles. The delayed BODIPY release of M(BDP/Pt) in vivo is consistent with the results of BODIPY release in vitro. The significant difference in NIR BODIPY release between M(BDP/Pt) and RGD-M(BDP/Pt) could be associated with the different pathway of endocytosis. Many reports have shown that receptor mediated endocytosis accelerated tumor cell uptake of RGD-decorated micelles.[31-33]

3.7 Anti-tumor efficacy

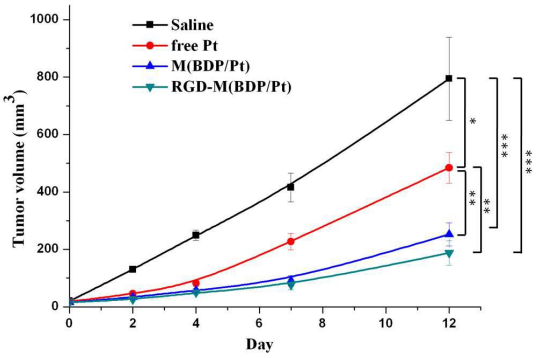

Fig. 7 In vivo anti-tumor efficacy evaluation of the drug-loaded micelles on EMT6 xenograft. The Pt injection was carried out on day 0, 2, 4 via tail vein at the dose of 5 mg Pt equivalent/kg body weight. Differences between groups were evaluated by analysis of variance (ANOVA) to demonstrate statistical significance ($P<0.05$)

The anti-tumor activity was performed on the xenograft EMT6 mouse mammary carcinoma. The tumor volume was measured and recorded for 12 days. As shown in Fig. 7, compared with saline, free CDDP and CDDP-loaded micelles showed obvious anti-tumor efficacy, and both micelles group showed better tumor inhibition. The cRGD decorated Pt-loaded micelles resulted in the best efficacy of tumor inhibition. At day 12, free CDDP, M(BDP/Pt) and RGD-M(BDP/Pt) got tumor suppression rate of 39.1%, 68.2% and 76.4%, respectively. The better anti-tumor efficacy of RGD-M(BDP/Pt) than untargeted micelles could be attributed to the more cellular uptake of Pt-loaded micelles as indicated by cell experiment in vitro.

4 Conclusion

In this study, multifunctional micelles by combining RGD targeting, near-infrared BODIPY imaging, and anticancer drug delivery were successfully developed. The BODIPY and RGD were conjugated to the pendant groups of dextran and the anticancer drug cisplatin was complexed with the pendant carboxyl groups of dextran. CLSM and live animal imaging analysis indicate preferred accumulations of dextran micelles in EMT6 breast cancer cells and breast cancer xenografts after cRGD decoration. Moreover, the dextran micelles displayed good anti-tumor efficacy in vivo. This work highlights the potential role of multifunctional theranostic micelles in tumor diagnosis and cancer therapy.

Acknowledgements
Financial support was provided by the Science and Technology Department of Jilin Province (Project no. 20111809, 20130624003JC, 2014866 and 20130206050YY), and National Natural Science Foundation of China (Project no. 81170632, 91227118, 51503003 and 51373167).

Notes and references

[a]*Life Science Research Center, Beihua University, Jilin 132013, P. R. China E-mail: sunxinbh@126.com;*
[b]*State Key Laboratory of Polymer Physics and Chemistry, Changchun Institute of Applied Chemistry, Chinese Academy of Sciences, 5625 Renmin Street, Changchun 130022, P. R. China*
[c]*School of Basic Medical Sciences, Beihua University, Jilin132013, P. R. China E-mail: bhdxgaixiaodong@126.com;*

1 M. Liong, J. Lu, M. Kovochich, T. Xia, S. G. Ruehm, A. E. Nel, F. Tamanoi and J. I. Zink, ACS nano, 2008, **2**, 889-896.
2 N. Sanvicens and M. P. Marco, Trends Biotechnol., 2008, **26**, 425-433.
3 K. Park, S. Lee, E. Kang, K. Kim, K. Choi and I. C. Kwon, Adv. Funct. Mater., 2009, **19**, 1553-1566.
4 Z. Cheng, A. Al Zaki, J. Z. Hui, V. R. Muzykantov and A. Tsourkas, Science, 2012, **338**, 903-910.
5 C. K. Huang, C. L. Lo, H. H. Chen and G. H. Hsiue, Adv. Funct. Mater., 2007, **17**, 2291-2297.
6 C. Oerlemans, W. Bult, M. Bos, G. Storm, J. F. W. Nijsen and W. E. Hennink, Pharmaceut. Res., 2010, **27**, 2569-2589.
7 M. Zheng, S. Liu, J. Li, D. Qu, H. Zhao, X. Guan, X. Hu, Z. Xie, X. Jing and Z. Sun, Adv. Mater., 2014, **26**, 3554-3560.
8 J. Yue, S. Liu, R. Wang, X. Hu, Z. Xie, Y. Huang and X. Jing, Mol. Pharmaceutics., 2012, **9**, 1919-1931.

9 R. Wang, X. Hu, J. Yue, W. Zhang, L. Cai, Z. Xie, Y. Huang and X. Jing, J. Mater. Chem. B., 2013, **1**, 293-301.
10 R. Wang, X. Hu, S. Wu, H. Xiao, H. Cai, Z. Xie, Y. Huang and X. Jing, Mol. Pharmaceutics., 2012, **9**, 3200-3208.
11 W. Song, Z. Tang, D. Zhang, Y. Zhang, H. Yu, M. Li, S. Lv, H. Sun, M. Deng and X. Chen, Biomaterials, 2014, **35**, 3005-3014.
12 P. Couvreur, Adv. Drug Delivery Rev., 2013, **65**, 21-23.
13. F. Alexis, E. M. Pridgen, R. Langer and O. C. Farokhzad, in Drug Delivery, Springer, 2010, pp. 55-86.
14 L. Brannon-Peppas and J. O. Blanchette, Adv. Drug Delivery Rev., 2012, **64**, Supplement, 206-212.
15 K. Kataoka, A. Harada and Y. Nagasaki, Adv. Drug Delivery Rev., 2011, **47**, 113-131.
16 J. Panyam and V. Labhasetwar, Adv. Drug Delivery Rev., 2012, **55**, 329-347.
17 X. Hu, J. Li, W. Lin, Y. Huang, X. Jing and Z. Xie, RSC Advances, 2014, **4**, 38405-38411.
18 K. Miyata, R. J. Christie and K. Kataoka, React. Funct. Polym., 2011, **71**, 227-234.
19 U. Kedar, P. Phutane, S. Shidhaye and V. Kadam, Nanomedicine (London, U. K.), 2010, **6**, 714-729.
20 J. Varshosaz, Expert Opin. Drug Delivery, 2012, **9,** 509-523.
21 Y.-Z. Du, Q. Weng, H. Yuan and F.-Q. Hu, ACS nano, 2010, **4**, 6894-6902.
22 B. Li, Q. Wang, X. Wang, C. Wang and X. Jiang, Carbohydr. Polym., 2013, **93**, 430-437.
23 L. Li, Z. Bai and P. A. Levkin, Biomaterials, 2013, **34**, 8504-8510.
24 Z. Zhao, Z. Zhang, L. Chen, Y. Cao, C. He and X. Chen, Langmuir, 2013, **29**, 13072-13080.
25 L. Yuan, W. Lin, K. Zheng, L. He and W. Huang, Chem. Soc. Rev., 2013, **42**, 622-661.
26 Y. Ni and J. Wu, Org. Biomol. Chem., 2014, **12**, 3774-3791.
27 J. Karolin, L. B. A. Johansson, L. Strandberg and T. Ny, J. Am. Chem. Soc., 1994, **116**, 7801-7806.
28 G. Ulrich, R. Ziessel and A. Harriman, Angew. Chem. Int. Ed., 2008, **47**, 1184-1201.
29 N. Jiang, J. Fan, T. Liu, J. Cao, B. Qiao, J. Wang, P. Gao and X. Peng, Chem. Commun., 2013, **49**, 10620-10622.
30 S. Zhu, J. Zhang, J. Janjanam, J. Bi, G. Vegesna, A. Tiwari, F.-T. Luo, J. Wei and H. Liu, Anal. Chim. Acta., 2013, **758**, 138-144.
31 Z. Zhen, W. Tang, H. Chen, X. Lin, T. Todd, G. Wang, T. Cowger, X. Chen and J. Xie, ACS nano, 2013, **7**, 4830-4837.
32 S. Kunjachan, R. Pola, F. Gremse, B. Theek, J. Ehling, D. Moeckel, B. Hermanns, M. Pechar, K. Ulbrich and W. E. Hennink, Nano. Lett., 2014, **14**, 972-981.
33 J. Yang, Y. Hou, G. Ji, Z. Song, Y. Liu, G. Dai, Y. Zhang and J. Chen, Eur. J. Pharm. Sci., 2014, **52**, 180-190.
34 H. Xiao, R. Qi, S. Liu, X. Hu, T. Duan, Y. Zheng, Y. Huang and X. Jing, Biomaterials, 2011, **32**, 7732-7739.
35 H. Xiao, H. Song, Q. Yang, H. Cai, R. Qi, L. Yan, S. Liu, Y. Zheng, Y. Huang and T. Liu, Biomaterials, 2012, **33**, 6507-6519.
36 H. Xiao, J. F. Stefanick, X. Jia, X. Jing, T. Kiziltepe, Y. Zhang and B. Bilgicer, Chem. Commun., 2013, **49,** 4809-4811.
37 L. Quan, S. Liu, T. Sun, X. Guan, W. Lin, Z. Xie, Y. Huang, Y. Wang and X. Jing, Acs. Appl. Mater. Interfaces., 2014, **6**, 16166-16173.
38 X. Hu, X. Guan, J. Li, Q. Pei, M. Liu, Z. Xie and X. Jing, Chem. Commun., 2014, **50**, 9188-9191.
39 M. Li, Z. Tang, S. Lv, W. Song, H. Hong, X. Jing, Y. Zhang and X. Chen, Biomaterials, 2014, **35**, 3851-3864.
40 Z. Li, M. Zheng, X. Guan, Z. Xie, Y. Huang and X. Jing, Nanoscale, 2014, **6**, 5662-5665.
41 F. Danhier, B. Vroman, N. Lecouturier, N. Crokart, V. Pourcelle, H. Freichels, C. Jerome, J. Marchand-Brynaert, O. Feron and V. Preat, J. Controlled Release., 2009, **140**, 166-173.

